RSC Advances

ROYAL SOCIETY OF CHEMISTRY

www.rsc.org/advances

Graphical Abstract

The ‘S’ atom of thiourea functionalized polystyrene adsorbent exhibited very strong interaction with excellent separation of antimony(III and V) ions in presence of large concentration of cobalt and zirconium ions.

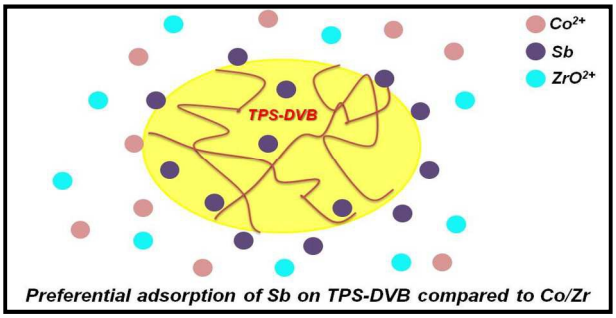

Experimental and DFT Studies for Selective Separation of Sb(III) and Sb(V) from Mixtures with Zr(IV)/Co(II) using Thiourea Grafted Polystyrene Adsorbent

Jyotsna S. Arora[1], Uttamkumar Joshi[1], Vilas G. Gaikar[1,*]

[1]Department of Chemical Engineering,

Institute of Chemical Technology,

Nathalal Parekh Marg,

Matunga, Mumbai 400019, India

and

Sk. Musharaf Ali[2]

[2]Chemical Engineering Division,

Bhabha Atomic Research Centre,

Mumbai 400 085, India

*Corresponding author: Tel.: +91-022-33612013; fax: +91-022-33611020;

e-mail ID: vg.gaikar@ictmumbai.edu.in

Abstract

A thiourea functionalized polystyrene adsorbent (TPS-DVB) is theoretically and experimentally investigated for selective sorption of antimony from acidic aqueous mixtures with $CoCl_2$ and $ZrOCl_2$. The optimal uptake of 35.6 and 24.2 $mg.g^{-1}$, respectively, was obtained for antimony(III) and antimony(V), at pH 1. The isotherm data could be well explained by the Langmuir model and the adsorption kinetics was successfully fitted in the *pseudo* first-order kinetics. Very high separation factors of 1129 and 918 were achieved for the Sb(III)/Co(II) and Sb(V)/Co(II) mixtures, respectively. The adsorption of Sb(III) and Sb(V) ions onto the TPS-DVB adsorbent was explored using the Density Functional Theory (DFT). These theoretical studies of metal coordination with the sulfur atom in the isothiourea group of the adsorbent showed stronger interaction of Sb(III) and Sb(V) ions over Co(II) and ZrO(II) ions. The inclusion of solvation model in the theoretical calculations improved the agreement between the experimental and the calculated metal-sulphur bond distances.

Keywords: zirconium, thiourea, adsorption, DFT, separation factor

1. Introduction

The zirconium (98%)-tin (1.5%) alloy is used as a structural cladding material in nuclear plants owing to its low cross-sectional area for capture of thermal neutrons and corrosion resistance.[1] Cobalt, < 20 $mg.kg^{-1}$, is present as an impurity in the zirconium-tin alloy.[1] The radionuclides, ^{58}Co and ^{125}Sb are formed as the activation products of cobalt and tin present in the cladding material. Several efforts have been directed to separate these radionuclides when dissolved in aqueous acidic solutions.[1-5] The current state-of-art separation processes are heavily dependent on inorganic adsorbents and ion exchangers.[4]

The oxidation state and co-ordination structures of metal ions in aqueous solutions play important roles in the formation of metal-extractant complex, thus enabling separation.[6] The aqueous acidic solutions of cladding material comprises of cobalt in +2 oxidation state, zirconium in +4 form while antimony exhibits two oxidation states (+3,+5).[1,2,4,7] Kumar *et al.*[8] reported selective sorption of Co(II), from aqueous HCl solutions of concentrated ZrO(II) ions, using *penta*-aza and *hexa*-aza macrocyclic ligands, starting with the molecular design of these ligands using Density Functional Theory (DFT) calculations. Bishay[3] has reported effective separation Co(II) and Sb(III) using Amberlite C-G 400 resin (separation factor , $\alpha_{Sb^{3+}/Co^{2+}} = 850$). Devi *et al.*[1] used Dowex 50-X8 and Dowex 1-X8 resins for adsorptive separation of radioactive ^{60}Co and ^{125}Sb ions. However, these ion exchange resins get loaded mainly with Zr because of their strong affinity for zirconium ions at 1-3 M acid concentrations, resulting in poor selectivity.[1,8] Further, the separation of antimony and cobalt using ion chromatography poses several processing problems[9,10] along with use of concentrated acid solutions (6-11 M)[1,3,5] for adsorption/elution and exhibiting little selectivity simultaneously.

The properties of a solid polymer matrix can be tailored to achieve the desired selectivity for separating a metal ion from the aqueous mixtures and operational flexibility[11] by selecting an available ligand or by designing a specific complexing molecule. The derivatization may alter the acid/base properties of the adsorbent as well as may help in the preorganisation of the ligands. Understanding the metal ion-ligand interaction becomes, therefore, necessary to design the metal selective adsorbents. Deorkar and Tavalarides[9] have used pyrogallol-silica gel ceramics in an adsorption column to separate Sb(III) from aqueous copper and lead salt solutions with the adsorption capacity of 5.0 mg Sb(III)/g of ceramics. Saito *et al.*[12] and Kawakita *et al.*[13] used porous hollow-fiber membrane containing N-methylglucamine (NMG) that gave uptake of 96 mg and 130 mg of Sb(III) and Sb(V), respectively per gram of the membrane.

According to Pearson's acid-base theory,[14] the chemical hardness or the softness of a metal ion may decide its selectivity and coordination properties toward a donor atom. Zr(IV) in ZrO(II) ion is classified as a hard acid, while Co(II) and Sb ions (III and V) are borderline and soft acids, respectively. Hence, taking advantage of this weak acidity of antimony, sulfur in thioether and thiols as soft base, is considered as the best choice for the donor atom. The S-containing organics,[15-18] mainly thiourea, have been reported for antimony complexation[19-23] and also as antimony eluting agent from ion exchange columns.[7,24] In addition, thiourea immobilized as thiol and isothiouronium resins have also been reported for selective removal of heavier transition metals.[25-30]

The current work reports the use of thiourea based polystyrene adsorbent (TPS-DVB) for selective and optimum adsorption of antimony(III and V) ions from mixtures with cobalt and zirconium. The DFT studies were also performed for the complexation of the metal ion with the functionalized adsorbent providing structural, energetics and electronic information.

2. Materials and Methods

2.1. Materials

Chloromethylated polystyrene (CMPS) beads cross-linked with 2% divinylbenzene, was obtained from Auchtel Pvt. Ltd. (Mumbai, India) with 3.5 *meq*/g of chlorine content. Thiourea, K_2CO_3 and tartaric acid (all AR-grade) were obtained from s.d. Fine Chemicals, Mumbai, India. Deionized water was used to prepare the stock solutions. The Sb(V) and Sb(III) stock solutions were prepared from potassium hexahydroxoantimonate(V) (Sigma-Aldrich, >99%) and antimony trichloride (Thomas baker, >99%), respectively, in aqueous HCl solutions. Cobalt chloride (s.d. Fine Chemicals) and zirconyl chloride (s.d. Fine Chemicals) were used for the preparation of cobalt and zirconium solutions. Standard solutions (ICP grade, 1000 $mg.dm^{-3}$) of Co, Zr and Sb were obtained from Sigma-Aldrich.

2.2. Methods

The carbon, hydrogen, nitrogen and sulphur contents of the adsorbent, after the grafting process, were analysed using a Perkin-Elmer 240B Elemental Analyser. A Bruker-VERTEX 80V FT-IR spectrophotometer, aligned with Ultra-Scan interferometer, was used to record the spectra of TPS-DVB with KBr pellets. Inductively coupled plasma atomic emission spectroscopy (ICP−AES) (ARCOS, MS Spectro, Kleve, Germany) was used to measure the metal-ion concentrations with an instrument detection limit (IDL) of 10 ppb for all metal ions. A radiofrequency (RF) generator with 1400 W power and 27.12 MHz frequency was used along with charge-coupled device (CCD). Argon gas was used as the nebulizer gas, auxiliary gas, and also for the generation of plasma with flow rates of 0.8, 1, and 12 $dm^3.min^{-1}$, respectively. The samples were injected into the plasma by maintaining the pump speed of 30 rpm. Post metal adsorption, the energy-dispersive X-ray analysis (EDX) by JEOL scanning electron microscope

was used for the elemental analysis of the polymer beads after coating with platinum. The accelerating voltage was 20-30 kV and the electric current was 15 mA.

3. Experimental and Computational Section

3.1. Experimental Section

3.1.1. Synthesis of thiourea grafted poly(styrene−DVB) resin (TPS-DVB)

The synthesis (*Scheme 1*) and characterization of thiourea grafted on poly(styrene−DVB) copolymer (TPS−DVB) was performed according to previous reports.[30,31]

***Scheme 1*: Synthesis of thiourea grafted adsorbent (TPS-DVB)**

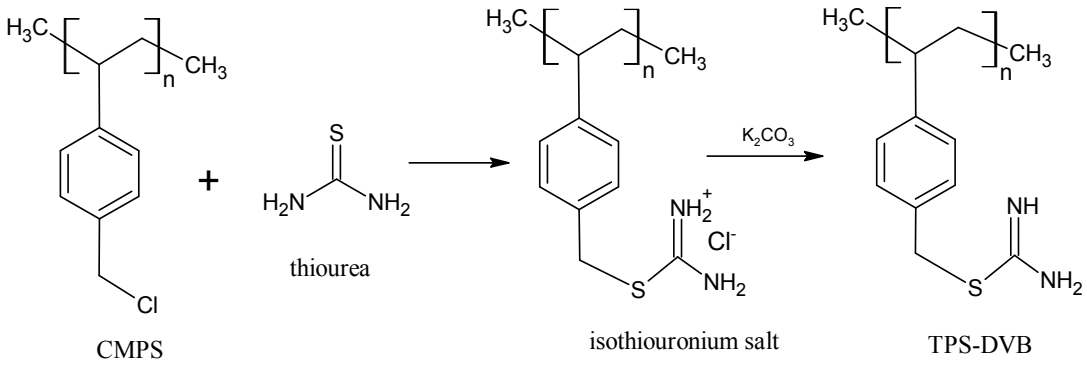

3.1.2. Batch Adsorption Studies

The competitive batch sorption of antimony ions (III and V) in the presence of cobalt and zirconium ions was investigated by suspending 20 mg of the adsorbent in stoppered conical flasks containing 10 cm^3 of solutions after adjusting the pH of the solution to an optimum value. The pH of the solution was adjusted by using dilute aqueous solutions of HCl or NaOH, each of 0.1 M concentration. The flasks were kept on an orbital shaker with an agitation rate of 100 $strokes.min^{-1}$ at an ambient temperature of 303 ± 2 K for 24 h equilibration. The residual metal-ion concentrations in the solutions were measured by ICP−AES.

The metal-ion uptake by the adsorbent was estimated from the difference in the initial and residual metal-ion concentrations (C_o and C_e, respectively) in the aqueous solutions. The adsorption capacity per unit weight of adsorbent, Q_{av}, (Eqn (1)) and percentage adsorption (%R) (Eqn (2)) were calculated as [30-32]

$$Q_{av} = \frac{(C_o - C_e) * V_s}{W_s} \quad (1)$$

$$\%R = \frac{(C_o - C_e)}{C_o} * 100 \quad (2)$$

where W_s is the weight of the solid adsorbent (g) and V_s is the volume of the solution (dm^3). The distribution coefficient, K_d ($dm^3.g^{-1}$) (Eqn (3)) was calculated as

$$K_d = \frac{(C_o - C_e) * V_s}{W_s * C_e} \quad (3)$$

and separation factor (α) is given by Eqn (4)

$$\alpha = \frac{K_{d,Sb}}{K_{d,Co}} \quad (4)$$

The kinetics of antimony(III) and antimony(V) adsorption was studied at 303 K and pH = 1 with 100 cm^3 (V_0) of 100 ppm initial antimony concentration and 200 mg of TPS-DVB. The samples (V_t) were withdrawn at regular intervals and an equal amount of 0.1 M HCl was added into the bulk solution so as to maintain the volume of the solution constant during the adsorption study. The metal uptake at any time t_i, $Q_{t,i}$ ($mg.g^{-1}$) is given by Eqn (5) [33]

$$Q_{t,i} = \frac{(C_0 - C_{t,i}) * V_0 - \sum_2^{i-1} C_{t,i-1} * V_t}{W_s} \quad (5)$$

where, $C_{t,i}$ is the metal concentration at any time t_i.

The desorption studies were performed by using 0.05 M tartaric acid and 0.1 M NaOH solution.[10] The metal loaded TPS-DVB was equilibrated with the eluent for 3 h. The adsorbent was then filtered and the resulting solution was acidified with dilute HCl solution prior to ICP-

AES analysis. The adsorbent was washed thoroughly with deionized water, dried at 363 K and was used in the subsequent three-cycle of adsorption–desorption experiments.

3.2. Computational Section

DFT studies on thiourea, TPS-DVB and the metal-adsorbent complexes in the presence of chloride counter-ions were performed for understanding the atomistic interactions between antimony, cobalt and zirconyl ions with TPS-DVB. The Gaussian *09* program[34] was used for investigating the structural and electronic properties. The B3LYP functional[20,35-38] with LANL2DZ-ECP basis set was considered for the metal ions[20,35-38]. The 6-311+G(*d,p*)[39] basis set was considered for the rest of the atoms as it was found to successfully predict various molecular properties. The geometry optimization of all the molecules was performed without imposing any initial symmetry restriction. The cobalt(II) ion (possessing three unpaired electrons) has quartet multiplicity while in all antimony(III), antimony(V) and zirconyl(II) ions, there are no unpaired electron. Hence for the simulation studies of Co(II)-TPS-DVB (weak ligand) complexes surrounded by chloride ions, unrestricted formalism (*viz.* UB3LYP) was employed. The absence of imaginary frequencies during the Hessian calculations characterized these as stationary points. For all the complexes, corrections to the interaction energy were calculated by considering the basis set superposition error (BSSE) with counterpoise correction (CPC)**.**[40]

Geometry optimization of the complexes including the solvent effects were further performed with the Integral Equation Formalism Polarized Continuum Model (IEFPCM)[41] in Gaussian *09*. The dielectric constant (ε) for bulk water was taken as 78.4 and Natural Bond Order (NBO) method was employed to calculate the natural population analysis.

4. Results and Discussion

The functional group loading, specific Brunauer-Emmett-Teller (BET) macropore surface area, average pore size and pore volume of TPS-DVB were measured in co-ordinance with our previous reports on the similar adsorbents.[30,31]

4.1. Equilibrium metal adsorption studies on TPS-DVB

The pH of the solution significantly affects the nature of functional groups on the adsorbent surface[31] and the speciation of metal ions.[10] The plots of single component adsorption of Sb(III) and Sb(V) on TPS-DVB as a function of pH are shown in Fig. 1. In the pH range of 0-2, a considerable change in the Q_{av} values were observed while the amount of antimony adsorbed was almost constant beyond pH = 4. The highest uptake of Sb(III) as well as that of Sb(V) occurs at pH 1 *viz.* 35.6 and 24.2 $mg.g^{-1}$, respectively. A similar adsorption behavior of the maximum uptake at pH 1 was reported for Sb(V) ions on pyrogallol bonded to silica gel ceramic support.[9] However, when the pH was increased from 2 to 6, antimony adsorption decreased significantly due to the formation of hydroxide species[7] ($Sb(OH)_3$ and $[Sb(OH)_6]^-$) in the solutions. Further, at pH conditions, below 1, thiourea leaches out from the polystyrene surface decreasing the adsorption capacity of TPS-DVB for Sb.[31]

To evaluate the selectivity of TPS-DVB for Sb ions from Co/Zr mixtures, competitive sorption experiments were performed at pH = 1 since TPS-DVB exhibited the highest adsorption capacity (Q_{av}) of Sb ions at this pH. It was noted that zirconium had almost negligible adsorption on TPS-DVB while cobalt to some extent showed an interaction, but antimony interacted very well with TPS-DVB. The adsorption constants, K_d , for Sb(III) and Co(II) from their binary mixtures are 1.242 and 0.0011 $dm^3.g^{-1}$, respectively while for Sb(V) and Co(II) mixtures the values are 1.010 and 0.0016 $dm^3.g^{-1}$, respectively (Table 1). The selectivity factor

(α) for Sb(III) and Co(II) mixtures is ($\alpha_{Sb(III)/Co}$) 1129 while that of Sb(V) and Co(II) mixtures ($\alpha_{Sb(V)/Co}$) is 918. These results clearly indicate much stronger interaction of Sb(III) and Sb(V) with TPS-DVB as compared to that of cobalt and zirconium. The bonding of the metal ions with TPS-DVB was further confirmed by elemental analysis using EDX. The peaks in the EDX spectrum at 2.31 and 6.92 keV correspond to the binding energies of SKa[31] and CoKa[42] (Fig. 2(a)), respectively, while peak at 3.60 keV corresponds to the binding energy of SbLa[43] (Fig. 2(b)).

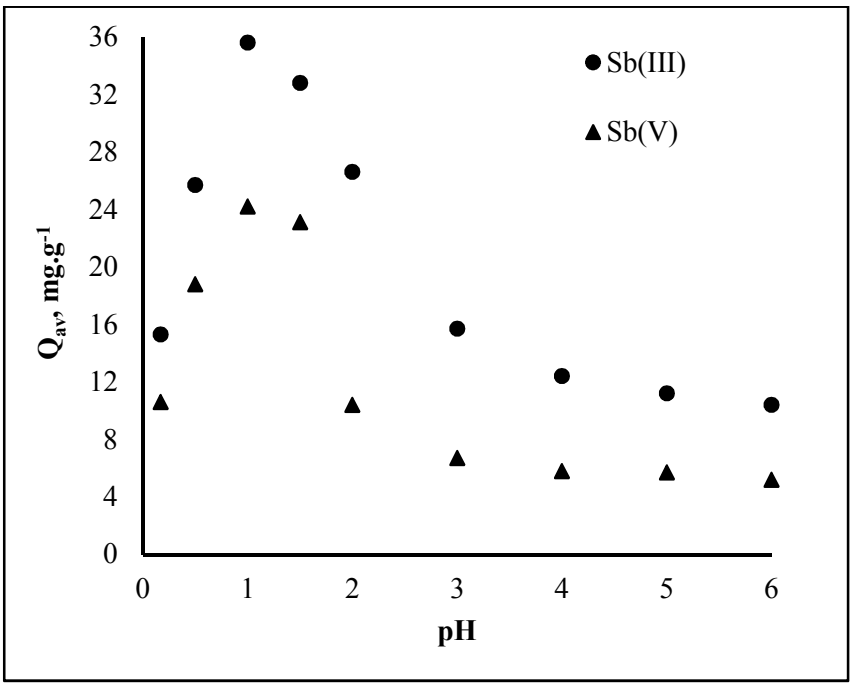

Figure 1: Effect of pH on sorption of Sb(III) and Sb(V)

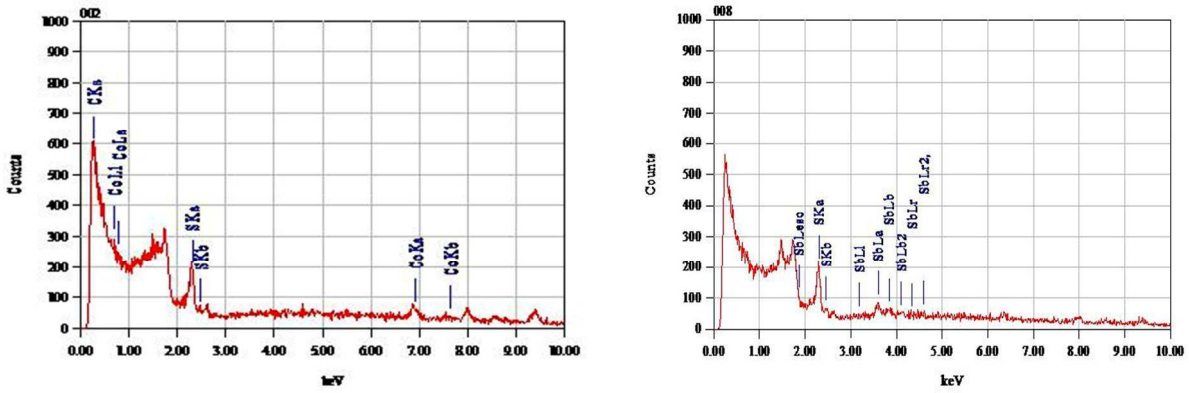

(a) **(b)**

Figure 2: EDX spectrum of Co (a) and Sb (b) on TPS-DVB after adsorption.

Table 1

Experimental results for co-adsorption of antimony and cobalt on TPS-DVB at pH = 1

Antimony					Cobalt					α
C_o; ppm	C_e; ppm	% R	Q_{av}; mg.g^{-1}	K_d; dm^3.g^{-1}	C_o; ppm	C_e; ppm	% R	Q_{av}; mg.g^{-1}	K_d; dm^3.g^{-1}	
Sb(III)										
96.9	27.8	71.31	34.55	1.242	472.1	471.1	0.21	0.50	0.0011	1129
Sb(V)										
71.6	23.7	66.89	23.95	1.010	472.1	470.6	0.32	0.75	0.0016	918

The experimental equilibrium adsorption data for the uptake of antimony and cobalt ions were further analyzed by Langmuir adsorption model (Eqn (6)) to estimate the maximum loading capacity of TPS-DVB.

$$Q_{av} = Q_{max} \cdot \frac{K_L C_e}{1 + K_L C_e} \quad (6)$$

where, Q_{max} is the maximum metal ion adsorption capacity per unit weight of adsorbent (mg.g^{-1}), C_e is metal ion concentration in the aqueous phase at equilibrium in ppm. K_L(dm^3.mg^{-1}) represents the Langmuir adsorption constant. The plots of Q_{av} of Sb(III), Sb(V) and Co(II) *vs.* C_e show that the Q_{max} for Sb(III) and Sb(V) as 40.01 and 25.64 mg.g^{-1} resin, respectively, as against 0.65 mg.g^{-1} resin for Co(II) (Fig. 3). These plots exhibit a good correlation between the experimental (Q_{exp}) and the Langmuir model (Q_{fit}) confirming monolayer coverage of metal ion on TPS-DVB surface.

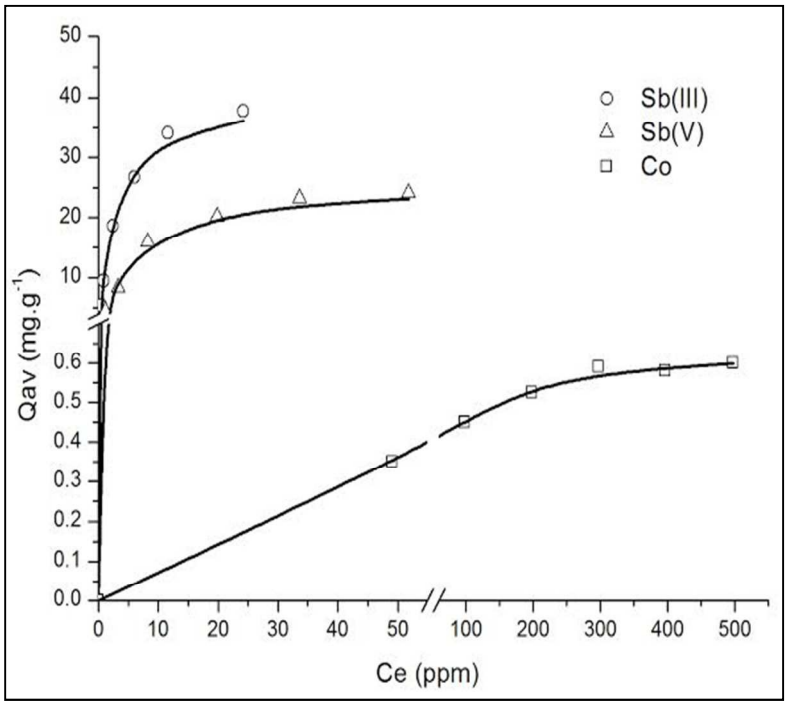

Figure 3: Effect of metal concentration on the adsorption density

The suitability of the adsorbent (R_L) for the uptake of metal ions can be determined by the Langmuir model described according to Eqn (7)[30],

$$R_L = \frac{1}{1+(K_L C_0)} \quad (7)$$

The R_L values for TPS-DVB for Co(II) and Sb (III as well as V) ions are less than one suggesting that TPS-DVB was suitable for adsorption of these metal ions. In addition, the spontaneity of the adsorption process can be elucidated from ΔG values which can be calculated according to Eqn (8)[33]

$$\Delta G = -RTlnK_L \quad (8)$$

where R ($J.mol^{-1}.K^{-1}$) is the gas constant, T (K) is the temperature, and K_L ($dm^3.mol^{-1}$) is the Langmuir constant. Table 2 also gives the ΔG values for the adsorption of antimony and cobalt ions by TPS-DVB at 303 K, suggesting their spontaneous adsorption.

The adsorption kinetics studies were also performed for the time-dependent uptake of both Sb(III) and Sb(V) ions. Initially, the adsorption rate is high and reaches 67 and 53%, for Sb(III) and Sb(V), respectively, within 5 h (Fig. 4). However, as time progresses, adsorption becomes slower and reaches the equilibrium values of 89 and 66%, for Sb(III) and Sb(V), respectively, after 24 h. Hence the solution was equilibrated for a minimum of 24 h. The experimental data was modeled using the *pseudo* first-order kinetics given by Eqn (9) and the Lagergren's plot[31] is given in Fig. 4 (inset).

$$\log(Q_e - Q_t) = \left(-\frac{k}{2.303}\right) t + \log Q_e \quad (9)$$

The kinetic parameters, Q_e value and the rate constant k are 30.70 $mg.g^{-1}$ and 0.36 h^{-1} for Sb(III) while 24.90 $mg.g^{-1}$ and 0.41 h^{-1} for Sb(V) ions. The adsorption kinetics is well represented by Lagergren's model as the calculated values are in agreement with the experimental data (Fig. 4 (inset)).

In order to show the reusability of TPS-DVB, the adsorbed metal was eluted with 0.1 M NaOH with 0.05 M tartaric acid mixture. After three consecutive cycles of adsorption-

desorption, the removal percentage was 67 and 60% for Sb(III) and Sb(V), respectively, *viz.* less than 12% decrease in the adsorption efficiency occurred.

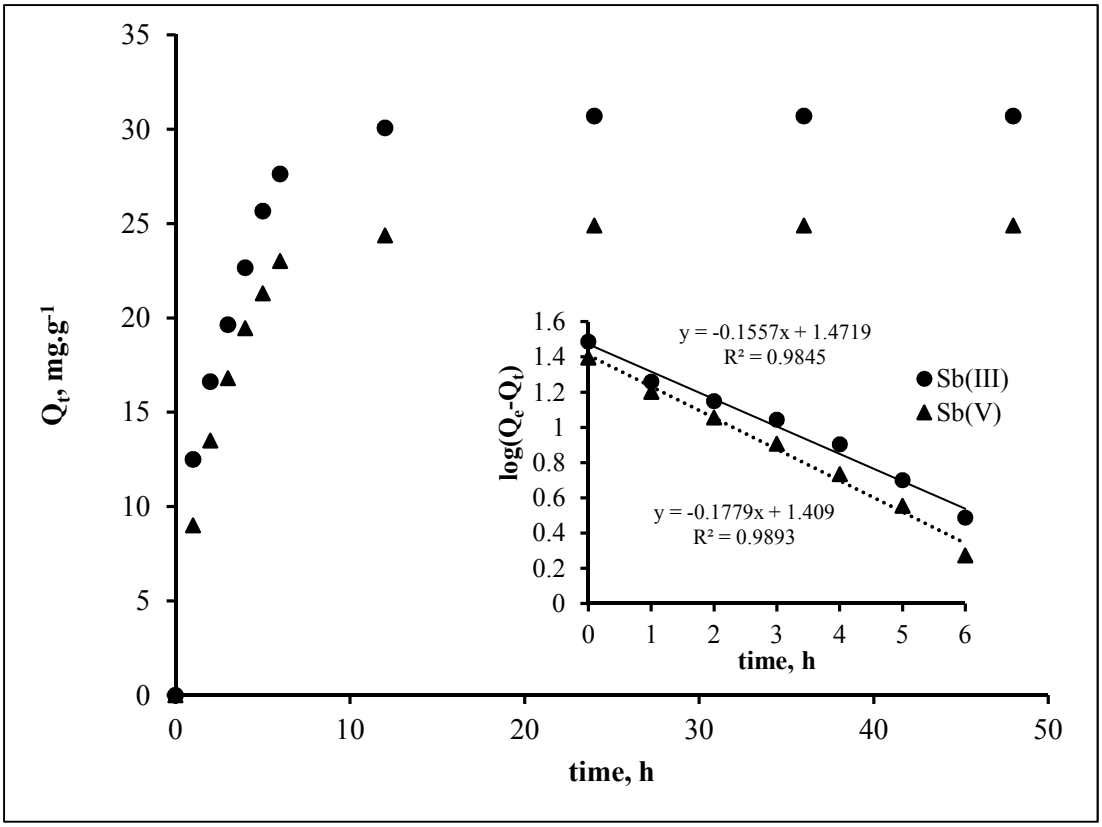

Figure 4: Effect of contact time on adsorption of antimony (inset: Lagergren's plot)

Table 2

Adsorption Constants Degree of Suitability Values and free energy change parameters for TPS-DVB

	Q_{max}; mg.g^{-1}	K_L; dm^3.mg^{-1}	R_L	ΔG, kJ.mol^{-1}
Sb(III)	40.01	0.39	0.19-0.03	-9.73
Sb(V)	25.64	0.18	0.36-0.53	-7.79
Co(II)	0.65	0.024	0.46-0.08	-0.86

4.2. Metal-adsorbent Coordination Mechanisms

The DFT calculations were performed to comprehend the fundamental atomic interactions between the functionalized adsorbent and the metal ion surrounded by counterions during the complexation studies.[44-46]

4.2.1. Structure and properties of thiourea and TPS-DVB

The DFT optimized structure of thiourea and its mapped electrostatic potential surface (MESP) are shown in Fig. 5(a) and 5(b), respectively. The 'S' in thiourea possesses two lone pairs of electrons considering its sp^2 hybridization and hence, the MESP has significant negative charge around 'S' atom which is capable of attracting metal ions. These calculated geometrical parameters are in close agreement with the reported experimental and computed values obtained at B3LYP/6-311++G** level (Table 3).[47] The orbital analysis of thiourea exhibit that the main atomic contributions to highest occupied molecular orbital (HOMO) of thiourea (Fig. 5(c))[48] come from 89% "*p*" character of sulfur while 73% "*p*" character of sulfur contributes towards the next occupied orbital (HOMO-1) (Fig. 5(d)). Hence, the HOMO and HOMO-1 are mostly constituted of a lone pair *3p* orbital contribution from 'S'. The simultaneous consideration of MESP surface and the two molecular orbitals, shows the hybridized lone pairs of 'S' (Fig. 5(e)). The arrow along the 'S-C' double bond indicates the direction along which the metal ion could approach 'S'. The complex formation with the metal ions is expected through π bonding as shown in Fig. 5(e).

For simplified molecular simulations, the thiourea grafted polystyrene resin (TPS-DVB) was represented as the isothiouronium group bonded to a benzyl group.[49] The DFT optimized structure of the grafted adsorbent is shown in Fig. 5(f) along with its MESP in Fig. 5(g) where the electron rich region is towards C=N group. *2p* orbitals of nitrogen are more radially

contracted and thus difficult to approach by the metal ion for bonding, while the lone pairs of 'S' are easily available for bonding with the metal ion. The HOMO of TPS-DVB (Fig. 5(h)) is mostly constituted of a lone pair orbital contribution from 'S' while the lowest unoccupied molecular orbital (LUMO) is localized mainly on the polystyrene backbone (Fig. 5(i)).The calculated geometrical parameters are given in Table 3. In addition, the calculated gas phase vibrational frequencies of TPS-DVB are in very good agreement with the experimental FTIR values (Table 3).

The HOMO-LUMO energy difference (E_{eg}) was calculated by using Eqn (10)

$$\text{HOMO} - \text{LUMO energy difference } (E_{eg}) = E_{LUMO} - E_{HOMO} \quad (10)$$

The calculated values of the frontier orbital energy difference $E_{eg,PCM}$ and $E_{eg,g}$ of TPS-DVB are 5.496 and 5.597 eV, respectively. The lower value of $E_{eg,PCM}$ than $E_{eg,g}$ is due to solvation. The orbitals of the ligand (isothiourea supported on polystyrene backbone) being less bulky get substantially influenced by the presence of surrounding medium (water in this case). This results in decreased frontier ligand orbital gap[36] $E_{eg,PCM}$ compared to the gas phase orbital gap $E_{eg,g}$.

Table 3

Comparison of experimental values with DFT optimized bond lengths and bond angles of thiourea and TPS-DVB.

Isothiourea				TPS-DVB			
						Vibrational frequency, cm^{-1}	
	Cal.	Cal.[47,a]	Exp.[47,b]			Cal.	Exp.
$r_{C\text{-}S,}$ Å	1.676	1.671	1.689	*$r_{Cb\text{-}S,}$ Å	1.863	701	702
				**$r_{CT\text{-}S,}$ Å	1.809		
$r_{C\text{-}N,}$ Å	1.359	1.365	1.329	$r_{C\text{-}N,}$ Å	1.382	1616	1615
				$r_{C=N,}$ Å	1.273		
$0.\theta_{S\text{-}C\text{-}N,}$	122.3	122.6	121.6	$\theta_{S\text{-}CT=N,}$ deg	122.9	$E_{eg} = E_{LUMO} - E_{HOMO,}$ eV	

deg	θ S-CT-N, deg	115.9	$E_{eg,g}$	5.597
	θ CT-S-Cb, deg	104.1	$E_{eg,PCM}$	5.496

[a] (B3LYP/ 6-311++G**)
[b] experimental values
[*] C_b is the C atom of benzyl group
[**] C_T is the C atom of thiourea moiety

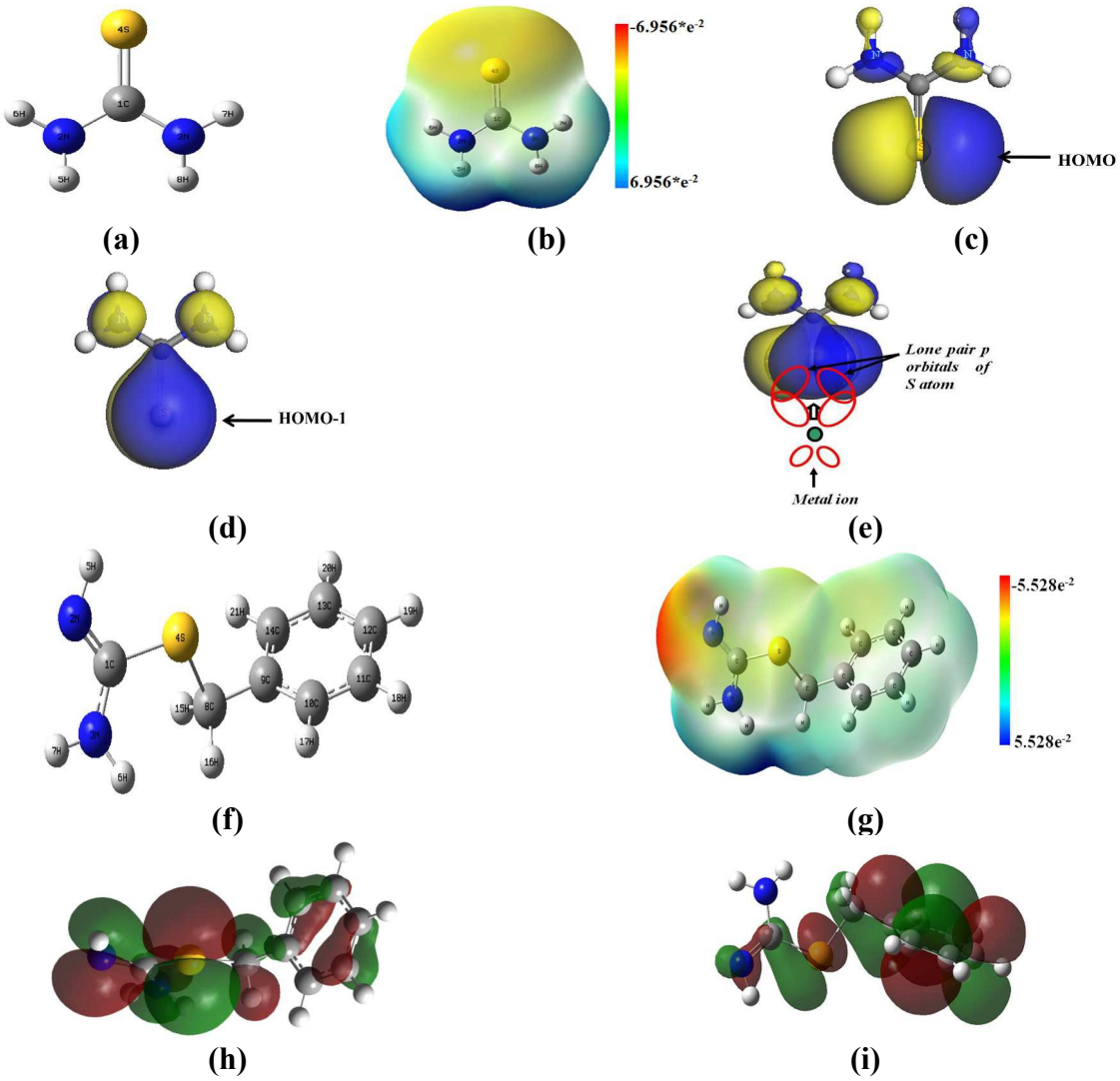

Figure 5: The DFT optimized structure of thiourea (a), its mapped electrostatic potential surface (MESP) (b), the Highest occupied (c) and the next occupied molecular orbitals of thiourea (d). The visualization of atomic lone pair orbitals of the S atom and the possible direction with mode of metal ion bonding is shown (e), the optimized TPS-DVB moiety (f), mapped electrostatic potential surface of TPS-DVB (g), the highest occupied (h) and the lowest unoccupied MOs (i) of TPS-DVB. The electron density around the S atom ranges from -2.01 to 2.11e^{-2}.

4.2.2. Interaction of TPS-DVB with Sb(III & V), Co(II) and Zr(IV)

The interaction between TPS-DVB and metal chlorides can be rationalized by the quantum chemical properties *viz.* electronegativity *(χ),* hardness *(η)* and the electrophilicity index *(ω)* as calculated by Eqn (13), (14) and (15), respectively. Pearson (2005)[50] stated that for an interacting system of two species differing in its electronegativities, the electronic flow will occur from the molecule with the lower electronegativity (the organic molecule) towards that of higher value (metal species). Further, a lower value of ω signifies a more reactive nucleophile while the converse is stated for an electrophile (high value of ω)[51]. The χ and ω values for all the species in the present study are listed in Table 4. These values indicate that the TPS-DVB adsorbent is nucleophilic and hence interact with the electrophilic metal chlorides.

$$\chi = \left(\frac{-(E_{LUMO} + E_{HOMO})}{2}\right) \quad (13)$$

$$\eta = E_{LUMO} - E_{HOMO} \quad (14)$$

$$\omega = \chi^2 \Big/ 2\eta \quad (15)$$

Table 4

Electronegativity and electrophilicity index values for metal chlorides and the adsorbents

	χ	ω
TPS-DVB	0.1375	0.0467
Sb(III)	0.2022	0.0930
Sb(V)	0.2004	0.0755
Co(II)	0.1794	0.0566
ZrO(II)	0.1709	0.0451

The gas phase interaction energy ΔE_G between the metal ion and TPS-DVB surrounded with counter-ions to maintain electroneutrality was calculated using Eqn (11) and are given in Table 5.[52]

$$\Delta E_G = E_{complex} - (E_{TPS-DVB} + E_{metal-chloride}) \quad (11)$$

where, E is the total energy of the respective optimized structures. The interaction energies of all the metal complexes with TPS-DVB and counter-ions are negative showing attractive interactions. The BSSE correction was also performed using by Eqn (12) and the BSSE corrected binding energy ΔE_{corr} and $(M-S)_G$ bond length are given in Table 5.

$$\Delta E_{corr} = \Delta E_{gas} + BSSE \quad (12)$$

From the gas phase calculations it is seen that, the effect of BSSE as well as the comparison of $(M-S)_G$ bond length with the experimental values, exhibit a discrepancy for antimony *viz*. the trend in ΔE_G was found to be reversed when compared to the experimental selectivity of metal ion adsorption (Table 5). Since, adsorption of the metal ion occurs from aqueous acidic solutions, the metal-adsorbent interaction is largely influenced by the presence of solvent molecules. Hence, the implicit solvation model was employed for the metal-counterion-TPS-DVB complexation.

The optimized structures of the adsorbent–metal complexes from solvation studies are shown in Fig. 6. The value of ΔE_{PCM} for Sb(III) is more negative than Sb(V) and Co(II) ions (Table 5) exhibiting an attractive interaction, while slightly positive ΔE_{PCM} was observed for ZrO(II) ion, thus exhibiting unfavorable interaction (Table 5). This indicates that Sb(III and V) gets selectively adsorbed on TPS-DVB due to their strongest interaction with S of TPS-DVB. The trend in interaction energy Sb(III) > Sb(V) > Co(II) > ZrO(II), is now consistent with the experimental adsorption data. Similarly, Hocking *et al.*[43] and Song *et al.*[45] inferred that favorable coordination between the chelating adsorbents and metal

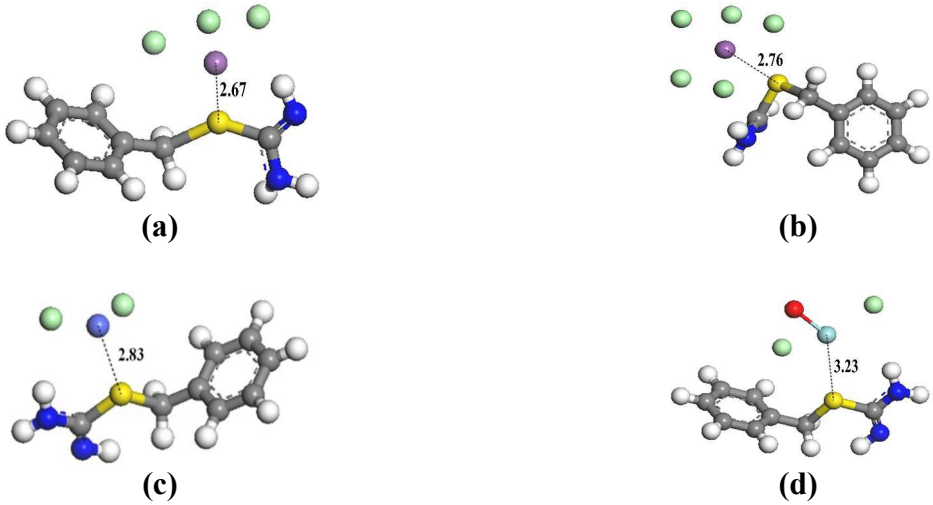

Figure 6: DFT optimized interaction of Sb^{3+} (a), Sb^{5+} (b), Co^{2+} (c) and ZrO^{2+} (d) with TPS-DVB and the counter-ions with implicit solvation model. The grey, blue, yellow, green, white, and red represents C, N, S, Cl, H, and O atoms, respectively. Sb, Co and Zr atoms are represented by purple, cyan and silver spheres, respectively.

Table 5

DFT optimized parameters for metal with TPS-DVB in gas phase as well as implicit solvation model.

Resin+metal+ Counter-ion	ΔE_{Gas}, kcal.mol^{-1}	$BSSE$, kcal.mol^{-1}	ΔE_{corr} kcal.mol^{-1}	$(M-S)_G$ (Å)	ΔE_{PCM}, kcal.mol^{-1}	$(M-S)_{PCM}$ (Å)	M-S$_{exp}$ (Å)
$[ZrO]^{2+}$	-29.99	2.99	-25.13	2.74	0.44	3.23	
Co^{2+}	-37.60	3.61	-31.79	2.46	-8.74	2.83	[a]2.35-2.37
Sb^{5+}	-13.05	3.14	-9.9	2.81	-12.42	2.76	[b]2.70-2.77
Sb^{3+}	-6.22	1.98	-4.24	2.92	-16.21	2.67	[c]2.52-2.79

[a]Silvestru *et al.* [53], [b]Sharutin *et al.*[54],[c]Ozturk *et al.*[20]

cations can be correctly evaluated by considering the solvation effect during DFT calculations. Further, the $M - S_{PCM}$ is the least for Sb(III) while the highest for ZrO(II). These calculated values of $(M - S)_{PCM}$ bond length are in good correlation with the reported XRD values.[20, 53,54]

The charge transfer values (Q_T) were calculated by summing up the NPA charges on metal chlorides in the adduct[8] and changes in the optimized geometrical parameters of TPS-DVB adsorbent post metal complexation are given in Table 6. For all the metal-adsorbent complexes, negative Q_T signifies flow of electrons from the lone pair of 'S' atom to metal ion which is consistent with the Pearson's acid-base theory.[14,50] Maximum charge transfer occurs in Sb(III) complex, followed by Sb(V), Co(II) and least for Zr(IV). On comparing the chemical groups of all the complexes, considerable distortions of bond lengths of TPS-DVB with Sb(III) and Sb(V) were observed. However, very little changes in TPS-DVB adsorbent post Co(II) and ZrO(II) complexation occurred confirming lesser interaction and lowered stability.

Table 6

Comparison of bond lengths, bond angle computed with implicit solvation model of TPS-DVB (before and after complexation) and charge transfer from TPS-DVB to metal.

	$r_{CT\text{-}S}$, Å	$r_{Cb\text{-}S}$, Å	$\theta\ C_T\text{-}S\text{-}C_b$, deg	Q_T (*e*)
TPS-DVB	1.805	1.862	105.61	
$[ZrO]^{2+}$	1.831	1.854	105.68	-0.159
Co^{2+}	1.837	1.831	105.72	-0.218
Sb^{5+}	1.877	1.828	105.98	-0.515
Sb^{3+}	1.886	1.825	106.12	-0.608

* C_b is the C atom of benzyl group, ** C_T is the C atom of thiourea moiety

Comparative study with Literature Reports

Although it is difficult to directly compare the adsorption efficiency of TPS-DVB with other adsorbents because of the different experimental conditions used, it is still apparent that the selectivity for antimony over cobalt is much higher with the current adsorbent at low acid concentrations than the reported ion exchanger adsorbents. Devi *et al.*[1] reported $\alpha_{Sb^{3+}/Co^{2+}} = 16$ for an anion exchanger Dowex 1-X8 with quaternary ammonium functional group in Cl^- form in 8 M HCl while the cation exchanger Dowex 50-X8 with sulfonic acid functional group, exhibited $\alpha_{Sb^{3+}/Co^{2+}} = 50$ in the presence of 9 M HCl. However, with 0.5 M HCl, the Dowex 1-X8 and Dowex 50-X8 resins exhibited selectivity towards cobalt with $\alpha_{Sb^{3+}/Co^{2+}} = 1.25$ and 0.06, respectively. These separation factors are at much lower level as compared to the TPS-DVB giving good separation factors which ensure very selective pick-up of antimony ions at low acid concentrations. Further, Bishay[3] reported the simultaneous adsorption of cobalt and antimony(III) from 8 M HCl solutions on an anion exchange column filled with Amberlite CG-400 resin having quaternary ammonium functional groups in Cl^- form. These metal ions are selectively eluted with 3 M HCl and 0.1 M $HClO_4$, respectively with $\alpha_{Sb^{3+}/Co^{2+}} = 850$. Though the separation of cobalt and antimony using the ion exchange process was effective, the major disadvantages of this process are the handling of highly concentrated solutions for adsorption and the nuclear waste streams contains other metal ions which might also get adsorbed on these non-selective resins.

The TPS-DVB adsorbent can overcome the demerits of the usual ion-exchange process resulting in effective separation of antimony from Co and Zr mixture. Further, DFT results are in agreement with the experimental data, indicating that DFT is helpful to determine the complexation of metal cations with the functionalized adsorbent.

5. Conclusions

Thiourea modified polymeric adsorbent having styrene backbone was evaluated as an excellent antimony selective adsorbent in the presence of cobalt and zirconium. The maximum adsorption capacity of the adsorbent for Sb(III) and Sb(V) was 40.01 and 25.64 $mg.g^{-1}$ with a high separation factor 1129 and 918, respectively. The results of DFT calculations on inclusion of solvation are in accordance with the experimental adsorption data. The HOMO is located on 'S' atom of TPS-DVB which interacts with the metal ion. The computed M-S bond distances (under solvation conditions) are in good agreement with the XRD values for similar systems.

Acknowledgements

We acknowledge the Department of Atomic Energy, Government of India, for the financial support and IITB SAIF, IITB Department of Earth Science, for the analytical support.

References

1. P. S. R. Devi, S. Joshi, R. Verma, A. V. R. Reddy, A. M. Lali and L. M. Gantayet, *Nucl. Technol.*, 2010, **171**, 220.
2. G. Stephenson, P. E. Skinner, and C. Jensen, EPRI International Low-Level Waste Conference, Albuquerque, NM, 2006.
3. T. Z. Bishay, *Anal. Chem.***,** 1972**, 44**(6), 1087.
4. R. Harjula, A. Paajanen, R. Koivula, E. Tusa and R. Kvarnström, WM2009 Conference, Phoenix, AZ, 2009.
5. H. Koshima, *Anal. Sci.,* 1986, **2**, 255.
6. R. D. Hancock and A. E. Martell, *Chem. Rev.,* 1989, **89**(8), 1875.
7. P. A. Riveros, *Hydrometallurgy*, 2010, **105**, 110.
8. P. Kumar, R. S. Madyal, U. Joshi and V. G. Gaikar, *Ind. Eng. Chem. Res.,* 2011, **50**, 8195.
9. N. V. Deorkar and L. L. Tavlarides, *Hydrometallurgy,* 1997, **46**, 121.
10. B. K. Biswas, J. Inoue, H. Kawakita, K. Ohto and K. Inoue, *J. Haz. Mat.,* 2009, **172**, 721.
11. A. R. Patil, J. S. Arora and V. G. Gaikar, *Sep. Sci. Technol.,* 2012, **47,** 1156.
12. T. Saito, H. Kawakita, K. Uezu, S. Tsuneda, A. Hirata, K. Saito, M. Tamada and T. Sugo, *J. Membr. Sci.*, 2004, **236**, 65.
13. H. Kawakita, K. Uezu, S. Tsuneda, K. Saito, M. Tamada and T. Sugo, *Hydrometallurgy,* 2006, **81**, 190.
14. R. G. Pearson, *J. Am. Chem. Soc.,* 1963**, 85,** 3533**.**
15. M. Wojciechowski, M. Piaścik and E. Bulska, *J. Anal. At. Spectrom.*, 2001, **16**, 99.
16. Z. Slovák and B. Dočekal, *Anal. Chim. Acta*, 1980, **117**, 293.

17. M. B. de la Calle-Guntinas, Y. Madrid and C. Cámara, *J. Anal. At. Spectrom.*, 1993, **8**, 745.
18. C. Bosch-Ojeda, F. Sánchez-Rojas, J. M. Cano-Pavón and L. Terrer-Martín, *Anal. Bioanal. Chem.*, 2005, **382**, 513.
19. A. Han, I. I. Ozturk, C. N. Banti, N. Kourkoumelis, M. Manoli, A. J. Tasiopoulos, A.M. Owczarzak, M. Kubicki and S. K. Hadjikakou, *Polyhedron*, 2014, **79**, 151.
20. I. I. Ozturk, N. Kourkoumelis, S. K. Hadjikakou, M. J. Manos, A. J. Tasiopoulos, I. S. Butler, J. Balzarini and N. Hadjiliadis, *J. Coord. Chem.*, 2011, **64**(22), 3859.
21. P. Smichowski, Y. Madrid and C. Cámara, *J. Anal. Chem*., 1998, **360**, 623.
22. M. Filella, N. Belzileb and Y. W. Chen, *Earth-Sci. Rev***.,** 2002, **59**, 265.
23. M. K. Upadhya and N. K. Udayashankar, *Can. J. Phys.,* 2009, **87**(4), 345.
24. *US Pat.,* 8 349 187 B2, 2013.
25. L. Wang, R. Xing, S. Liu, H. Yu, Y. Qin, K. Li, J. Feng, R. Li and P. Li, *J. Haz. Mat.,* 2010, **180**, 577.
26. X. Liang, Y. Xu, G. Sun, L. Wang, Y. Sun and X. Qin, *Colloids and Surfaces A: Physicochem. Eng. Aspects,* 2009, **349**, 61.
27. A. Warshawsky, M. M. B. Fieberg, P. Mihalik, T. G. Murphy and Y. B. Ras, *Separ. Purif. Method*, 1980, **9**(2), 209.
28. *US Pat.,* 4 561 947, 1985.
29. B. Saha, M. Iglesias, I. W. Dimming and M. Streat**,** *Solvent Extr. Ion Exc.*, 2000, **18**(1), 133.
30. P. Kumar, K. B. Ansari and V. G. Gaikar, *Ind. Eng. Chem. Res.,* 2012, **51**, 14209.

31. P. Kumar, K. B. Ansari, A. C. Koli and V. G. Gaikar, *Ind. Eng. Chem. Res.,* 2013, **52**, 6438.

32. Ö. Ercan and A. Aydin, *J. Braz. Chem. Soc.,* 2013, **24**(5), 865.

33. H. Yan, H. Li, X. Tao, K. Li, H. Yang, A. Li, S. Xiao and R. Cheng, *ACS Appl. Mater. Interfaces,* 2014, **6,** 9871.

34. M. J. Frisch, G. W. Trucks, H. B. Schlegel, G. E. Scuseria, M. A. Robb, J. R. Cheeseman, G. Scalmani, V. Barone, B. Mennucci, G. A. Petersson, H. Nakatsuji, M. Caricato, X. Li, H. P. Hratchian, A. F. Izmaylov, J. Bloino, G. Zheng, J. L. Sonnenberg, M. Hada, M. Ehara, K. Toyota, R. Fukuda, J. Hasegawa, M. Ishida, T. Nakajima, Y. Honda, O. Kitao, H. Nakai, T. Vreven, J. A. Montgomery, Jr., J. E. Peralta, F. Ogliaro, M. Bearpark, J. J. Heyd, E. Brothers, K. N. Kudin, V. N. Staroverov, R. Kobayashi, J. Normand, K. Raghavachari, A. Rendell, J. C. Burant, S. S. Iyengar, J. Tomasi, M. Cossi, N. Rega, J. M. Millam, M. Klene, J. E. Knox, J. B. Cross, V. Bakken, C. Adamo, J. Jaramillo, R. Gomperts, R. E. Stratmann, O. Yazyev, A. J. Austin, R. Cammi, C. Pomelli, J. W. Ochterski, R. L. Martin, K. Morokuma, V. G. Zakrzewski, G. A. Voth, P. Salvador, J. J. Dannenberg, S. Dapprich, A. D. Daniels, Ö. Farkas, J. B. Foresman, J. V. Ortiz, J. Cioslowski and D. J. Fox, GAUSSIAN 09 (Revision B.01), Gaussian Inc., Wallingford CT, 2009.

35. B. W. Walker, C. E. Check, K. C. Lobring, C. A. Pommerening and L. S. Sunderlin, *J. Am. Soc. Mass Spectrom.,* 2002, **13**, 469.

36. M. Maleki, F. Salimi, A. Shafaghat and M. K. Moghaddam, *Der Chemica Sinica*, 2012, **3**(3), 766.

37. G. G. Krishna, R. S. Reddy, P. Raghunath, K. Bhanuprakash, M. L. Kantam and B. M. Choudary, *J. Phys. Chem. B,* 2004**, 108**, 6112.

38. N. Rao, M. N. Holerca, M. L. Klein and V. Pophristic, *J. Phys. Chem. A,* 2007**, 111**, 11395.

39. E. P. A. Couzijn, J. C. Slootweg, A. W. Ehlers and K. Lammertsma, *J. Am. Chem. Soc.,* 2010, **132**, 18127.

40. L. Valenzano, B. Civalleri, S. Chavan, G. T. Palomino, C. O. Areán and S. Bordiga, *J. Phys. Chem. C,* 2010, **114,** 11185.

41. R. K. Hocking, R. J. Deeth and T. W. Hambley, *Inorg. Chem.,* 2007, **46**, 8238.

42. P. R. Martins, S. H. Toma, M. Nakamura, H. E. Toma and K. Araki, *RSC Adv.*, 2013, **3**, 20261.

43. A. Dailly, J. Ghanbaja, P. Willmann and D. Billaud, *Electrochim. Acta*, 2003, **48**, 977.

44. T. Mihaylov, N. Trendafilova, I. Kostova, I. Georgieva and G. Bauer, *Chem. Phys.,* 2006, **327**, 209.

45. L. Song, X. Zhao, J. Fu, X. Wang, Y. Sheng and X. Liu, *J. Haz. Mat.,* 2012, **199-200**, 433.

46. J. Gao, F. Liu, P. Ling, J. Lei, L. Li, C. Li and A. Li, *Chem. Eng. J.,* 2013, **222**, 240.

47. Z. Weiqun, Y. Wen and Q. Lihua, *J. Mol. Struc.-THEOCHEM*, 2005, **730**, 133.

48. F. Kandemirli and S. Sagdinc, *Corros. Sci.*, 2007, **49**, 2118.

49. R. S. Madyal and J. S. Arora, *RSC Adv.*, 2014, **4**, 20323.

50. R.G. Pearson, *J. Chem. Sci.*, 2005, **117** (5), 369.

51. A. Vektariene, G. Vektaris, and J. Svoboda, ARKIVOC, 2009, **7**, 311.

52. R. Sellin and S. D. Alexandratos, *Ind. Eng. Chem. Res.,* 2013, **52**, 11792.

53.

54. C. Silvestru, R. Rösler, R. Cea-Olivares, I. Haiduc and G. Espinosa-Pérez, *Inorg. Chem.,* 1995, **34**, 3352.

55. V. V. Sharutin, O. K. Sharutin, T. P. Platonova, A. P. Pakusina, D. B. Krivolapov, A. T. Gubaidullin and I. A. Litvinov, *Russ. J. General Chem*., 2002, **72**(9), 1379.

56. D. J. Williams, P. H. Poor, G. Ramirez and D. Vanderveer, *Inorg. Chim. Acta.*, 1989, 165, 167.

57. E. Hough and D. G. Nicholson, *J. Chem. Soc., Dalton Trans.,* 1981, 2083.